VO2 films obtained by V2O5 nanoparticle suspension reduction

Shian Guan, Manuel Gaudon, Aline Rougier, Etienne Duguet, Etienne Durand, Alexandre Fargues, Oudomsack Viraphong, Nicolas Penin

VO_2 films obtained by V_2O_5 nanoparticle suspension reduction

Shian Guan, Manuel Gaudon, Aline Rougier, Etienne Duguet, Etienne Durand, Alexandre Fargues,

*Oudomsack Viraphong, Nicolas Penin**

Univ. Bordeaux, CNRS, Bordeaux INP, ICMCB, UMR 5026, F-33600 Pessac, France

*Corresponding author: nicolas.penin@icmcb.cnrs.fr

Abstract

Applications of vanadium dioxide, VO_2, able to modulate near-infrared radiation by changing from a transparent to a reflective/absorptive state, remain limited by its shaping as transparent films. In this work, a V_2O_5@PVP core-shell structure is designed prior to the formation of island-structured VO_2 films. Poly(N-vinyl-2-pyrrolidone) (PVP) is used as a surface stabilizer for the preparation of V_2O_5 NP suspensions; additionally, PVP acts as a reducing agent during the film post-annealing process, helping the $V_2O_5 \rightarrow VO_2$ transformation under dynamic vacuum. Using *in situ* TG-FTIR characterization, the reducing mechanism is carefully discussed and analyzed. Finally, a uniform VO_2 film is fabricated with an attractive gray color and excellent thermal stability. Three strategies with various sintering parameters are used to optimize the film's morphology, *i.e.,* surface coverage. In the last strategy, the thermochromic behavior of the designed island-structure VO_2 film is simulated based on Mie scattering theory in consideration of surface coverage and "island" particle size fitting with our experiments. This pioneering work provides guidance for future studies on discontinuous VO_2 films.

1. Introduction

The design of improved energy-saving materials is an active research topic in materials science because of the increasing concern related to energy consumption and sustainable development. Building energy accounts for 30-40% of total energy consumption in developed countries, which is larger than that for industry or transportation. [1, 2] Approximately 50% of this energy comes from heating, ventilation and air conditioning systems. [2] Among various solutions to decrease energy consumption, smart windows based on chromogenic materials known for being able to modulate their optical properties under an external stimulus are being developed. As a representative thermochromic material, vanadium dioxide (VO_2) is component of smart windows that can respond to environmental temperature and modulate near-infrared irradiation (NIR) by changing from a transparent state at low temperature to a more reflective/absorptive state at high temperature,

corresponding to the monoclinic M and rutile R phases, respectively. [1, 3, 4, 5] The main difficulty besides such applications is the elaboration of thin films combining sufficient transparency in the visible region and high infrared absorption contrast depending on the M and R forms.

Over the past decade, several methods have been developed to fabricate VO_2-based films. [1, 4-10] Depending on the film morphology, continuous and discontinuous films are distinguished. Several experimental and simulation studies have indicated that discontinuous films, such as nanocomposite foils and nanoporous films, have superior properties, combining high luminous transmittance (T_{lum}) and high solar transmittance modulation (ΔT_{sol}), *i.e.,* better properties than VO_2-thin and continuous solid films (such as single layer or multiple layers by RF sputtering). [1, 4, 11, 12] Most investigations relied on VO_2-based composite films, *i.e.,* VO_2 nanoparticles (NPs) dispersed in various host materials, *e.g.,* polyurethane. [4, 12]

The fabrication of discontinuous films requires accurate surface engineering, including incorporating particles, tuning the porosity, designing nanocomposites, developing biomimetic patterns and creating grids. [1, 8, 13] To design two-dimensional patterned microstructures, several techniques have been investigated, such as photolithography, electron beam lithography, and colloidal lithography. [7, 14, 15] For example, using a colloidal crystal template made of a monolayer of polystyrene spheres, Ke *et al*. [14] modified the nanosphere lithography method and produced diverse patterned VO_2 films with tunable periodicity and nanostructures. [13, 16] Furthermore, 2D photonic crystal VO_2 films were shown to exhibit visible light tunability at room temperature and strong NIR modulation versus temperature. [16] Wang *et al.* [17] reported acid etching and self-patterning for discontinuous film fabrication. Introducing air as a secondary component into VO_2 (M) films is also a feasible alternative approach to achieve favorable T_{lum} and ΔT_{sol} simultaneously. Zhou *et al.* concluded on reduced optical constants with enhanced luminous transmittance for a nanoporous VO_2 film. [8] However, all film-shaping techniques usually suffer from low efficiency and high costs or the use of templates (masks or colloids).

In addition to the morphology issue, VO_2 (M) films suffer from rapid oxidation to V_2O_5 after being heated at 300°C in air, [6] evidencing poor thermal stability. This instability results in serious durability limitations in practical applications, requiring extra encapsulation processes. To improve the stability of VO_2 NPs, Gao *et al.* [18] reported a novel all-solution process through the preparation of VO_2@SiO_2 core-shell nanocrystals, where the SiO_2 shell serves as a protective layer to restrain oxygen diffusion and prevent the oxidation of the thermodynamically unstable VO_2 phase. A similar core-shell structure was also fabricated by Jin's group. Using microemulsion technology, [19] the prepared $V_{1-x}W_xO_2$@SiO_2 nanostructures could stand at 300°C for 2 h in air. Meanwhile, it should be noted that the process to prepare a core-shell structure is not easy to control. Furthermore, this treatment step leads to the aggregation of well-dispersed VO_2 NPs. Due to VO_2 poor crystallinity and the occurrence of traces of vanadium (+V) oxide, these fabricated VO_2-based films typically demonstrate an undesired brownish-yellow color. [4, 12, 18, 19] Generally, a colorless coating or coloration with light gray/blue light is more desirable.

Herein, we report a template-free surface-patterning method to fabricate discontinuous VO_2 films with NP arrays or island structures. As both a reducing agent and steric surface

stabilizer for NPs, we used poly(N-vinyl-2-pyrrolidone) (PVP), a synthetic vinyl polymer with a unique combination of properties, such as good solubility (in aqueous media), remarkable capacity to interact with a wide variety of organic and inorganic compounds, nontoxicity to living tissues, *etc*. [18, 20, 21] PVP indeed served as a surface stabilizer for the preparation of a well-dispersed V_2O_5 NP suspension and as a reducing agent during the post-annealing process performed under dynamic vacuum thanks to a homemade vacuum system leading to VO_2 film formation. Indeed, carbon was also previously reported as an efficient reducing agent for the synthesis of VO_2 powder through reducing V_2O_5 under dynamic vacuum. [22] To address the thermal stability of the as-prepared VO_2-based films, a high annealing temperature (700°C) was applied to increase their crystallinity. The obtained VO_2 film shows a visible homogeneous state with an attractive gray color and excellent thermal stability. Finally, regarding the "island"-like morphology of the prepared films, some optical simulations were performed with the consideration of various surface coverages and/or "island" sizes.

2. Experimental procedure

2.1 Preparation of V_2O_5 NPs

All reagents are analytical grade and used without further purification. V_2O_5 is homemade by heating vanadyl ethylene glycolate (VEG) at 300°C for 90 min in air. [23] Then, the obtained V_2O_5 NPs are mixed with soot (mole ratio 1: 1) and ball milled at a speed of 400 rpm for 1 h. Here, nanoscale soot (~35 nm) is used to destroy the rectangular shape of V_2O_5 particles initiated from the VEG template. It should be pointed out that the addition of soot is essential, as ball milling of pure V_2O_5 (without soot) fails to produce NPs with adequate shape for dispersion into chloroform suspensions. Then, the mixture is annealed in air (500°C for 30 min) to remove the excess carbon.

2.2 Preparation of V_2O_5@PVP suspension

The V_2O_5 NPs are pretreated with PVP (MW= 40 000, Sigma-Aldrich) in chloroform for 1 h under vigorous stirring, leading to a yellowish suspension of V_2O_5@PVP NPs. Different suspensions are prepared by varying the PVP/V_2O_5 weight ratio (R= 0, 0.64, 3.2 and 6.4) and V_2O_5 concentrations (C=20, 40, 80 and 160 g/L).

2.3 Fabrication of V_2O_5@PVP films and VO_2 films

The prepared V_2O_5@PVP suspensions are dropped onto quartz substrates and spin-coated (1000 rpm for 30 s). Next, the V_2O_5@PVP films are transferred into a homemade dynamic vacuum system (DVS) and annealed at 700°C for 15 h (heating rate of 10°C/min) to achieve homogeneous VO_2 films. Pumping is maintained throughout the annealing process.

2.4 Characterization

The surface morphologies of the as-prepared particles and films are observed by scanning electron microscopy (SEM) using a TESCAN Vega II SBH microscope and JEOL JSM-6700F and by high resolution transmission electron microscopy (HRTEM, JEOL 2200FS, operating at 200 kV). The carbon content is determined by a CHNS elementary analyzer (Thermo Fisher Scientific). The particle size in suspension is measured by laser diffraction for particle size analysis (Mastersizer 2000). The crystal structures of the as-prepared films are determined by X-ray diffraction (XRD) analyses (Philips PW1820, PANalytical X' Pert PRO MPD

diffractometer) using a Cu-Kα1 radiation source (λ=1.54056 Å) for room-temperature analyses and a cobalt K (α) radiation source (λ=1.78901 nm) for *in situ* measurements versus temperature. The film thickness is measured by a Dektak 32 Stylus Surface Profiler.

TG–FTIR measurements are performed with a TG Setsys "Evo" apparatus from Setaram Instrumentation coupled online to an FTIR Thermo Nicolet 380 spectrometer. Films are heated from 298 to 973 K at a rate of 2 K/min in a dry nitrogen atmosphere. IR spectra are recorded in the spectral range of 4400-740 cm^{-1} with a 2 cm^{-1} resolution and 32 scans.

3. Results and Discussion

3.1 Suspension preparation

With the help of the soot and ball milling process, V_2O_5 NPs with adequate size and shape (~185 nm) were successfully prepared (**Figure 1a**). The carbon excess was removed by heating in air, and the carbon content decreased from 6.4 wt% before annealing to 0.1 wt% after annealing, corresponding to a complete burnt of the soot.

It is still difficult to maintain nanosized particles in an organic liquid medium due to the formation and growth of aggregates, which are usually controlled by both interfacial chemical reactions and particle transport mechanisms. Aggregates up to several microns in size can be formed. Obviously, the formation of large aggregates impedes the formation of a stable suspension. Thus, PVP is used as a surface stabilizer to treat V_2O_5 NPs to avoid aggregate formation. The PVP polymer can be adsorbed onto different metal oxides (such as kaolinite, titania, iron oxide, alumina, and vanadium dioxide [18]), and it can stabilize NPs in water and many nonaqueous solvents. [24] Chloroform ($CHCl_3$) was chosen as solvent for PVP. Indeed, solvents with low boiling points allow thin films with homogeneous thickness to be obtained in agreement with a fast gelification process.

Figure 1c shows the particle size distribution in the suspensions prepared from different R = PVP/V_2O_5 weight ratios. Without PVP (R=0), microscale aggregates with a size of ~2.2 μm are observed. After functionalization with PVP (R=0.64 or over), the average particle size in the suspensions decreased to ~160 nm, which was basically consistent with the average diameter of V_2O_5 NPs extracted from SEM measurements (**Figure 1a**). PVP acts as a protective shell on each single V_2O_5 particle **(Figure 1b)** and avoids the formation of aggregates. Thus, a core-shell structure, V_2O_5@PVP, is assumed to be formed. To further confirm this core-shell structure, high-resolution transmission electron microscopy (HRTEM) images were collected for V_2O_5 (R=0) and V_2O_5@PVP suspensions (R=0.64). Without the use of PVP, **Figures 1d,e** show V_2O_5 particles of 160 nm forming isotropic aggregates of 1 μm size **(Figure 1d)** or a necklace-type network (**Figure 1e**). This aggregation phenomenon is in good agreement with the particle size distribution in the suspension measured with the Mastersizer particle size analyzer. In comparison, no aggregates were observed after PVP functionalization. Furthermore, the particles display an unclear contour (**Figure 1f**), and this blurred contour cannot be improved through the adjustment of the TEM instrument. Thus, the PVP polymer is probably well coated on V_2O_5 NP surfaces. Further magnification shows that V_2O_5 NPs are encapsulated by a layered structure with a thickness of ~2.5 nm (inset **Figure 1f**). PVP serves as a surface stabilizer for V_2O_5 NPs and prevents the aggregation of

NPs *via* repulsive forces and the steric effect that arise from its hydrophobic carbon chains. Stable V_2O_5 suspensions with R=0 and R=0.64 are used for spin-coating in the following step.

3.2 VO_2 film preparation

Two V_2O_5 suspensions (R=0 and 0.64) were spin-coated on quartz substrates to prepare V_2O_5 and V_2O_5@PVP films.

3.2.1 Morphology study

The comparison of the SEM images of the V_2O_5 and V_2O_5@PVP films shows a drastic improvement in the film morphology with PVP addition **(Figure 2)**. Without PVP, the V_2O_5 film displays micron-sized aggregates (**Figure 2a**). With the addition of PVP into the V_2O_5 suspension, the as-prepared V_2O_5@PVP films exhibit a quite smooth morphology (**Figure 2b**), and some well-separated NPs are also visible and distributed on the surface. The crack-free morphology results from the good wettability of the suspension containing PVP on the substrate. V_2O_5@PVP films exhibit a bright orange color with good uniformity.

In this work, PVP not only acts as a surface stabilizer and binder in the preparation of the V_2O_5 suspensions but also as a reducing agent leading to the reduction from the V_2O_5 film to the VO_2 film during post-annealing treatments. In an earlier work, the reduction of V_2O_5 into VO_2 by carbon addition was successfully demonstrated using a homemade dynamic vacuum system. [22] Herein, the PVP polymer was used as a highly efficient carbon source for coating V_2O_5 NPs. Based on calculations, the molar C/V_2O_5 ratio necessary to entirely transform V_2O_5 in VO_2 is 1:7, while the R wt.% ratio PVP/V_2O_5 is 0.64. Therefore, it was believed that in our set of experiments, the PVP content was largely enough for the complete transformation of V_2O_5 into VO_2. The excess PVP was probably degraded after the high-temperature annealing treatment. In addition, this hypothesis does not consider PVP to be reduced but only as a carbon source. **Figure 3a** briefly summarizes the VO_2 film fabrication.

After annealing at 700°C for 15 h, the V_2O_5@PVP film color changed from orange to transparent gray (**Figure 3b**) while maintaining an acceptable visible transmittance with good uniformity. In comparison to the commonly reported yellow-brownish color, *i.e.,* signature of the existence of V^{5+} ions, the light gray color of VO_2 film suggests high purity of the prepared VO_2 films with the single presence of V^{4+}. [4, 12]

The VO_2 film displays a “zero-dimensional” monolayer morphology with isolated VO_2 islands randomly distributed on the substrate (**Figure 3c**). Specifically, the particle adopts a combination of elliptical-like and spherical shapes. VO_2 is formed as individual particles rather than as continuous films. While increasing the annealing temperature, the progressive softening of PVP favors the mobility of adjacent particles that can coalesce, leading to the formation of large “islands.” EDS analysis confirms the presence of the characteristic peaks of O, V, and Si for the islands (Spot B), while only Si and O signals are detected at spot A, corresponding to the quartz substrate (**Figure 3e**). The film thickness deduced from the cross-section SEM image (**Figure 3e**) is approximately 1.5 μm.

3.2.2 Structural study

Prior studies on the synthesis of VO_2 powder demonstrated high purity of the VO_2 phase for

an annealing temperature of 700°C [22]. The XRD diagrams of the quartz substrate, chosen for its high stability at temperature (**Figure 4**), indicate that it remains amorphous (i.e., has a very broad peak) even after being annealed at 700°C. Starting from the V_2O_5@PVP suspension (R= 0.64), the XRD diagram of the spin-coated bright yellow film consists of peaks of weak intensity corresponding to V_2O_5. After annealing, the XRD diagram of the VO_2 film represented by two peaks located at 2Θ= 27.8° and 57.5° that can be indexed as the (011) and (022) peaks of monoclinic VO_2 validates the efficiency of the V_2O_5@PVP core-shell structure for the reduction in VO_2. The existence of any additional peaks confirms the film purity.

The observation of a strong preferred orientation for a film coated on an amorphous substrate was rather surprising. In addition, such a phenomenon usually occurs at higher temperatures, for which a greater mobility of the growth species is observed. In the literature, using a well-chosen crystallized substrate, the control of some epitaxial growth for VO_2 thin films has previously been reported. For example, Paik *et al.* [13] reported nanocrystalline VO_2 films with a preferred orientation (011), synthesized through rapid thermal annealing transformation of VO_x nanocrystals. Such preferential orientation is also observed in films deposited on fused quartz and c-cut sapphire. Sahana *et al*. [25] described a strong (200) orientation for VO_2 films deposited by metal-organic CVD;

Nevertheless, in this work, the observation of a clear crystallographic orientation for VO_2 films is surprising from the use of a noncrystalline substrate (quartz). Furthermore, the observation of such a drastic orientation is also surprising in regard to the isotropic morphology of the vanadium oxide grains, which exhibit isotropic shapes.

3.2.3 Reaction mechanism

The transformation from V_2O_5 to VO_2 was followed by *in situ* TG-FTIR analysis. As it is impossible to apply dynamic vacuum during the TGA-FTIR measurement, an inert gas flow (N_2) was used.

The thermogravimetric curves of the PVP polymer show a degradation process occurring at approximately 425℃ (**Figure 5a)**. In agreement with the literature, the formation of vinyl pyrrolidone (VP) monomer in the main evolved volatile product was confirmed by FTIR (**Figure 5b**) [24]. The decomposition thermogram of the V_2O_5@PVP sample shows two additional peaks located at 305°C and 350°C prior to PVP degradation at 420°C. They are associated with the presence of two peaks at 2360 and 2311 cm^{-1} in the FTIR spectra assigned to CO_2/CO **(Figure 5b)**. After TG-FTIR measurement, a V_2O_3 powder was recovered, as confirmed by XRD (not shown here).

Thus, we assume two reduction processes take place in the N_2 flow. At 305°C, PVP provides the carbon source [C], and acting as the reductive agent, V_2O_5 is reduced in VO_2, as illustrated by the V_2O_5+[C]→$2VO_2$+CO/CO_2 equation. At 350°C, the generated CO gas acts as a more active reducing agent, and VO_2 is further reduced to V_2O_3. As schematized by the equation, $2VO_2$+CO→V_2O_3+CO_2. The sum of the weight changes is Δw/w%= 8.80% // Δw/w%= 9.65. Overall, the ratio of weight changes during the two stages is 0.91 (8.80%/9.65%). The value is almost the same as that obtained from the TGA test (0.90, 4.48%/4.98%). From this perspective, we deduce that V_2O_5 is first reduced to VO_2 at 305°C and then further reduced to V_2O_3 at 350°C. For thin film preparation, our homemade dynamic vacuum system (DVS) was used for the thermal treatment, and a pure VO_2 film without any traces of the V_2O_3

phase was evidenced by X-ray diffraction. We have interpreted the differences in the redox reactions of the V_2O_5@PVP samples during the TGA measurements under N_2 atmosphere and during thermal treatment using DVS, from the fact that using DVS, CO gas is pumped out as soon as it forms, which avoids the second-step reduction as well as the V_2O_3 formation observed in TGA analyses.

3.3 VO_2 phase transition

The M/R phase transition of the as-prepared VO_2 film was followed by *in situ* XRD with temperature. The evolution of the *in situ* XRD patterns from 25°C to 90°C is shown in **Figure 6a**. In the inset, the 31 to 34° region corresponding either to the 011 peak of the monoclinic phase at low temperature and to the 110 peak of the rutile phase at high temperature and the 48 to 51° region are magnified. In the heating cycle from 25 to 90°C, the (011) single peak at the angle of 32.5° shifts to a lower value, which could be ascribed either to the phase transition R→M or to the thermal expansion or both. The doublet peak at approximately 49.5° clearly transforms into a single peak associated with the R phase (with the increase in the unit-cell symmetry). When the temperature cools back to 25°C, the VO_2 (M) phase is recovered.

The corresponding transmittance at a wavelength of 2500 nm was recorded in the cooling and heating cycles in the range of 30-100°C (blue line in **Figure 6b)**. For practical reasons, the temperature cycle was started with a cooling half cycle from 90°C, and then, the heating half cycle was applied (red line in **Figure 6b).**

During the cooling cycle, globally, there is a jump of approximately 2-3% around the cooling transition close to 45°C. During the heating cycle, a sudden drop occurs at approximately 85°C in the transmittance-time curve. This clearly illustrates thermochromic behavior, and the transition temperature (T_c) is roughly determined to be 65°C. At high temperatures ($T>T_c$), the VO_2 film exists as a rutile phase with a high transmittance in the infrared region, while at low temperatures ($T<T_c$), a phase transition occurs from rutile to monoclinic VO_2(M), and then the film displays a low transmittance. Although the transmittance contrast is quite low, the evolution of the heating and cooling half temperatures to 45 and 85°C, respectively, *i.e.,* with a hysteresis width of approximately 40°C, is in good agreement with our earlier results reported on VO_2 powder. [22]

3.4 Thermal stability test

The thermal instability of VO_2, which [6] can be easily oxidized into V_2O_5 under some mild conditions (300°C+2 h in air), especially in the presence of moisture, would result in serious durability problems in practical applications. In our case, the VO_2 (M) phase remained stable after 2 h and even after 24 h of heating at 300°C in air (**Figure 7**), revealing excellent thermal stability. Such behavior is probably associated with the high crystallinity of VO_2 fabricated on the substrate thanks to the high annealing temperature (700°C). However, as the temperature increases to 400°C, small peaks characteristic of V_2O_5 appear, while those of VO_2 completely disappear. **Figure 7** reveals a great improvement in the VO_2 film thermal stability, meaning that the obtained VO_2 films could bear temperatures as high as 300°C. In comparison with the VO_2-SiO_2 core-shell structure to prevent VO_2 from being oxidized,

increasing the crystallinity is a quite easy and efficient way to increase the film thermal resistance. [22, 23]

3.5 Morphology optimization

The morphology of VO_2 films is of paramount importance to reach the desired optical and thermochromic properties. From the zero-dimensional monolayer morphology with an isolated island structure **(Figure 3b)**, the surface coverage (SC%, defined below) is used as a key criterion. A higher SC% should improve the optical transmittance modulation ability (specifically in the NIR region), while it would induce a negative effect on the visible transparency of the film.

$$Surface\ coverage\ (\mathrm{SC\%}) = \frac{S(VO_2)}{S(substrate) + S(VO_2)}$$

To increase the SC% and to produce denser VO_2 films, three strategies were applied under a fixed V_2O_5 and PVP ratio (R= 0.64), namely, (i) increasing the concentration of V_2O_5@PVP suspension for spin-coating, (ii) increasing the number of V_2O_5@PVP layers by repeating the spin-coating before a single annealing, and (iii) increasing the number of VO_2 film layers by repeating the spin-coating/annealing times (*i.e.,* performing intermediate annealing treatment between each new coating step). The details are listed in **Table 1**.

Specifically, for the first strategy, the V_2O_5 concentrations were set as 20, 40, 80 and 160 g/L in $CHCl_3$ solvent. The as-prepared V_2O_5@PVP films are transparent with a bright yellow color (**Figure 8a**). Obviously, the C160H sample is the darkest in color because of its highest V_2O_5 content leading to the worst transparency. The theoretical V_2O_5@PVP film thickness, y_h, is linked to the kinematic viscosity, *v*, of the solution and the rotation rate, *w,* of the spin coater apparatus. $y_h = 3.6(\mathrm{v}/w)^{0.5}$. [27] Even when the rotation rate is fixed at 1000 rpm, an increase in the V_2O_5@PVP concentration would lead to an increase in the viscosity of the suspension and thus the obtained film thickness. The thicknesses were measured by profilometry thanks to a diamond sensor apparatus. The V_2O_5@PVP film thickness increases from 1.0 μm (C20H) to 1.6 μm (C40H), 2.1 μm (C80H) and 4.6 μm (C160H), following a softer way than the V_2O_5@PVP concentration.

For the second strategy, the V_2O_5@PVP film layers were set as 2 and 4 layers by spin-coating the suspension (C40H), *i.e.,* two or four successive coatings were made, and after 700°C annealing, the obtained samples were named C40-L2 and C40-L4. The film thicknesses are 2.1 and 3.9 μm, respectively.

For the third strategy, between successive spin-coating depositions from the suspension (C80), an annealing treatment was performed. The obtained samples are named C80-AT2 or C80-AT3 depending on the number of successive VO_2 layers (2 or 3 layers, respectively). Among them, the AT2 and AT3 films show the darkest gray/blue color, and the visible transparency is degraded, as illustrated in **Figure 8c**.

The top-view SEM micrographs reported in **Figure 9** confirm that, as expected, all obtained VO_2 films exhibit a zero-dimensional island-like structure. The following two parameters were analyzed specifically: surface coverage (SC%) and “island” particle size (d). There is a strong relationship between the island size and the film thickness.

The SC% was determined by treatment of the SEM images (with ImageJ tool) and is shown in **Figure 10a**. The results basically meet our expectation, and all three strategies lead to an increase in the SC%. As the V_2O_5@PVP suspension concentration increases from 40 to 80 g/L, the SC% largely increases from 28.5% (C40H) to 42.5% (C80H). In addition, when the spin-coating time of the V_2O_5@PVP suspension (C= 40 g/L) increases to 4, it remains at 38.3% (L4). Furthermore, the SC% is nearly twice that for sample AT3 through increasing the spin-coating/annealing times in comparison with the reference single layer (C80H) prepared from the same suspension (C80). Consequently, the transparency of the VO_2 film worsens for C80-AT2 or C80-AT3.

More accurately, the simultaneous increases in both the "island" size and the SC% suggest a correlation. In **Figure 10b,** the "island size" distribution is split into three size populations: <0.3, between 0.4-0.6 and >1.0 μm. For the C80H film corresponding to a single coating, the majority (66%) of the VO_2 "island" shows a size below 0.3 μm. Approximately 22% of VO_2 lies in the size range of 0.4-0.5 μm, indicating partial agglomeration and sintering during the annealing process. For the AT2 and AT3 samples, the "island" size largely increases as SC%, especially for C80-AT3. 15% of the "islands" display a size over 1.0 μm. On a macroscopic point of view, *i.e.,* on the film homogeneity evaluation from simple human eye investigation, the various particle distributions are without any effect.

3.6 Optical simulation

To further guide our experimental approach and determine the impact of the island size and surface coverage on the infrared contrast between the M and R phases, simulation of the optical transmittance using the Mie calculator software was carried out. A scheme summarizing our set of simulation steps is illustrated in **Figure 11a**. Island-like VO_2 particles are surrounded and covered by an air layer, meaning that the light would be scattered. In this case, the following two parameters were considered for the determination of VO_2 film performance: surface coverage (SC%) and "island" size (d).

When a beam of light passes through the medium, the beam is quickly "attenuated" or weakened. The transmittance (T%) can be calculated with the following equation:

$$T = e^{-(TAC \times d)}$$

where TAC is shortened as the total attenuation coefficient, and d is the film thickness or particle diameter in our case.

The TAC value can be obtained through the Mie scattering calculator program. Other parameters are also needed, including sphere diameter (d), wavelength, index of fraction (IF) in the medium (IF_{air}= 1), real index of sphere, complex index of refraction, and concentration (c, spheres per cubic micron).

The real and complex index of refraction of VO_2 spheres at different wavelengths, called optical constants (n and k, respectively), can be obtained from the references, [29, 30] as summarized in the supporting information (**Table 1**). In addition, the concentration is defined as:

$$c = \frac{N(VO_2)}{V(Air) + V(VO_2)} = \frac{4SC\%}{\pi \times d^3}$$

The simulated results are summarized in **Figures 11b-11d**. First, the SC% is fixed at 40%, and the particle size (d) varies from 0.1 to 1 μm. Different optical behaviors are observed (**Figure 11b**). In the visible range, the film transparency worsened as the particle size increased from 0.1 to 0.3 μm or larger. In addition, the film with an oversized "island" (d= 1 μm) almost loses transmittance modulation ability. Overall, the film (d= 0.3 μm) shows a wider and larger optical modulation in the infrared region (1000-2500 nm).

Then, d is fixed at 0.3 μm, and SC% is adjusted from 10% to 80%. **Figure 11c** shows a similar optical behavior with an overall downshift in the visible region as SC% increases, decreasing down to values close to zero. Meanwhile, the transmittance modulation window in the near-infrared region becomes increasingly wider. Furthermore, at 500 nm, the modulation in transmittance between the monoclinic T_M and the rutile phase T_R ($\Delta T\% = T_M - T_R$) remains close to zero, while at 2000 nm, it increases with SC% to reach values of approximately 40% for an SC of 100% (**Figure 11d)**. A trade-off must be found between the film transparency at 500 nm and the modulation in transmittance at 200 nm.

Our simulations suggest that the "island" size plays a more significant role in the transmittance behaviors than the SC%. Preliminary experimental investigations indicate poor optical performances, showing that the real behavior of VO_2 films is much more complex. However, the simulation shows some guidance for future improvement. Deeper experimental work devoted to the optimization of the film morphology is still necessary to maintain the smallest particle size while increasing the surface coverage SC%.

4. Conclusion

In this work, we developed a new method for the fabrication of discontinuous VO_2 films with island-structure morphology. Here, PVP polymer was used as a surface stabilizer and reducing agent. Starting from V_2O_5 NPs, a colloidally stable V_2O_5@PVP suspension was prepared, followed by a reduction process during annealing. Thanks to the homemade dynamic vacuum system, V_2O_5 was quantitatively reduced to VO_2. A pure VO_2 film was fabricated with a consumer-acceptable gray color. The surface coverage of VO_2 was modulated through three simple strategies. Furthermore, with Mie scattering theory, the simulation of the thermochromic performance of the VO_2 film shows some guidance for future work by improving the film's morphology, namely, large surface coverage with small particle size.

Conflicts of interest

There are no conflicts to declare.

Acknowledgments

Shian Guan was supported by a grant from the China Scholarship Council. The authors would like to thank Eric Lebraud, Sonia Buffière, and Laetitia Etienne, for their assistance during the XRD, SEM & TEM, CHNS & particle size distribution studies. All authors contributed to the discussions and revisions of the manuscript.

References

[1] Y. Cui, Y. Ke, C. Liu, Z. Chen, N. Wang, L. Zhang, Y. Zhou, S. Wang, Y. Gao, Y. Long., Thermochromic VO_2 for energy-efficient smart windows, Joule 2 (2019) 1707-1746.

[2] Y. Ke, C. Zhou, Y. Zhou, S. Wang, S. H. Chan, Y. Long, Emerging thermal-responsive materials and integrated techniques targeting the energy-efficient smart window application, Adv. Funct. Mater. (2018) 1800113.

[3] Z. Yang, C. Ko, S. Ramanathan, Oxide electronics utilizing ultrafast metal-insulator transitions, Annu. Rev. Mater. Res. 41 (2011) 337-67.

[4]. F. Xu , X. Cao, H. Luo, P. Jin, Recent advances in VO_2-based thermochromic composites for smart windows, J. Mater. Chem. C 6 (2018) 1903-1919.

[5]. P. Ashok, Yogesh Singh Chauhan, Amit Verma, High infrared reflectance modulation in VO_2 films synthesized on glass and ITO coated glass substrates using atmospheric oxidation of vanadium, Opt. Mater. 110 (2020) 110438.

[6] G. Fu, A. Polity, N. Volbers, B. Meyer, Annealing effects on VO_2 thin films deposited by reactive sputtering, Thin Solid Films 515 (2006) 2519-2522.

[7] M. Liu, B. Su, Y. V. Kaneti, Z. Chen, Y. Tang, Y. Yuan, Y. Gao, L. Jiang, X. Jiang, A. Yu, Dual-Phase transformation: spontaneous self-template surface-patterning strategy for ultra-transparent VO_2 solar modulating coatings, ACS Nano 11 (2017) 407-415.

[8] M. Zhou, J. Bao, M. Tao, R. Zhu, Y. Lin, X. Zhang, Y. Xie, Periodic porous thermochromic VO_2 (M) films with enhanced visible transmittance, Chem. Commun. 49 (2013) 6021-6023.

[9] L. Kang, Y. Gao, H. Luo, Z. Chen, J. Du, Z. Zhang, Nanoporous thermochromic VO_2 films with low optical constants, enhanced luminous transmittance and thermochromic properties, ACS Appl. Mater. Interfaces 3 (2011) 135-138.

[10] A. Maaza, K. Bouziane, J. Maritz, D.S. McLachlan, R. Swanepool, J.M. Frigerio, M. Every Direct production of thermochromic VO_2 thin film coatings by pulsed laser ablation, Opt. Mater. 15 (2000) 41.

[11] J. Faucheu, E. Bourgeat-Lami, V. Prevot, A review of vanadium dioxide as an actor of nanothermochromism: challenges and perspectives for polymer nanocomposites, Adv. Eng. Mater. 21 (2019) 1800438.

[12] Z. Chen, Y. Gao, L. Kang, C. Cao, S. Chen, H. Luo, Fine crystalline VO_2 NPs: synthesis, abnormal phase transition temperatures and excellent optical properties of a derived VO_2 nanocomposite foil, J. Mater. Chem. *A* 2 (2014) 2718-2727.

[13] T. Paik, S. H. Hong, E. A. Gaulding, H. Caglayan, T. R. Gordon, N. Engheta, C. R. Kagan, C. B. Murray, Solution-processed phase-change VO_2 metamaterials from colloidal vanadium oxide (VO_x) nanocrystals, ACS Nano 8 (2014) 797-806.

[14] Y. Ke, X. Wen, D. Zhao, R. Che, Q. Xiong, Y. Long, Controllable fabrication of two-dimensional patterned VO_2 nanoparticle, nanodome, and nanonet arrays with tunable temperature-dependent localized surface plasmon resonance, ACS Nano 11 (2017) 7542-7551.

[15] C. Li, L. Qi, Colloidal-crystal-assisted patterning of crystalline materials, Adv. Mater. 22 (2010) 1494-1497.

[16] Y. Ke, I. Balin, N. Wang, Q. Lu, A. I. Y. Tok, T. J. White, S. Magdassi, I. Abdulhalim, Y. Long., Two-dimensional SiO_2/VO_2 photonic crystals with statically visible and dynamically infrared modulated for smart window deployment, ACS Appl. Mater. Interfaces. 8 (2016) 33112-33120.

[17] N. Wang, Y. K. Peh, S. Magdassi, Y. Long., Surface engineering on continuous VO_2 thin films to improve thermochromic properties: top-down acid etching and bottom-up self-patterning, J. Colloid. Interf. Sci. 512 (2018) 529-535.

[18] Y. Gao, S. Wang, H. Luo, L. Dai, C. Cao, Y. Liu, Z. Chen, M. Kanehira, Enhanced chemical stability of VO_2 nanoparticles by the formation of SiO_2/VO_2 core/shell structures and the application to transparent and flexible VO_2-based composite foils with excellent thermochromic properties for solar heat control, Energy Environ. Sci. 5 (2012) 6104-6110.

[19] Y. Zhou, A. Huang, Y. Li, S. Ji, Y. Gao, P. Jin, Surface plasmon resonance induced excellent solar control for $VO_2@SiO_2$ nanorods-based thermochromic foils, Nanoscale 5 (2013) 9208-9213.

[20] K. M. Koczkur, S. Mourdikoudis, L. Polavarapu, S. E. Skrabalak., Polyvinylpyrrolidone (PVP) in nanoparticle synthesis, Dalton. Trans. 44 (**2015**) 17883-17905.

[21] C. Graf, D. L. J. Vossen, A. Imhof, A. V. Blaaderen, A general method to coat colloidal particles with silica, Langmuir 19 (2003) 6693-6700.

[22] S. Guan, M. Gaudon, M. S. Basiège, O. Viraphong, N. Penin, A. Rougier, Carbon-reduction as an easy route for the synthesis of VO_2 (M1) and further Al, Ti doping, Dalton Trans. 48 (2019) 3080-3089.

[23] S. Guan, A. Rougier, O. Viraphong, D. Denux, N. Penin, M. Gaudon, Two-Step synthesis of VO_2 (M) with tuned crystallinity, Inorg. Chem. 57 (2018) 8857-8865.

[24]. S. Haesuwannakij, T. Kimura, Y. Furutani, K. Okumura, K. Kokubo, T. Sakata, H, Yumi Yakiyama, H. Sakurai, The Impact of the polymer chain length on the catalytic activity of poly(*N*-vinyl-2-pyrrolidone)-supported gold nanoclusters, Scientific Reports 7 (2017) 9579.

[25] M. Sahana, M. Dharmaprakash, S. Shivashankar., Microstructure and properties of VO_2 thin films deposited by MOCVD from vanadyl acetylacetonate, J. Mater. Chem. 12 (2002) 333-338.

[26] M. I. Loria-Bastarrachea, W. Herrera-Kao, J. V. Cauich-Rodriguez, J. M. Cervantes-Uc, H. Vazquez-Torres, A. Avila-Ortega. A TG/FTIR study on the thermal degradation of poly(vinyl pyrrolidone), J. Therm. Anal. Calorim. 104 (2011) 737-742.

[27] M. V. Kelso, N. K. Mahenderkar, Q. Chen, J. Z. Tubbesing, J. A. Switzer. Spin coating epitaxial films, Science, 364 (2019) 166-169.

[28] C. Boragno, F. B. Mongeot, R. Felici, I. K. Robinson, Critical thickness for the agglomeration of thin metal films, Physical Review B 79 (2009) 155443.

[29] S. Li, G. A. Niklasson, C. G. Granqvist, Nanothermochromics: calculations for VO_2 nanoparticles in dielectric hosts show much improved luminous transmittance and solar energy transmittance modulation, J. Appl. Phys. 108 (2010) 063525.

[30] S. Li, G. A. Niklasson, C. G. Granqvist, Thermochromic undoped and Mg-doped VO_2 thin films and nanoparticles optical properties and performance limits for energy efficient windows. J. Applied Physics 115 (2014) 053513.

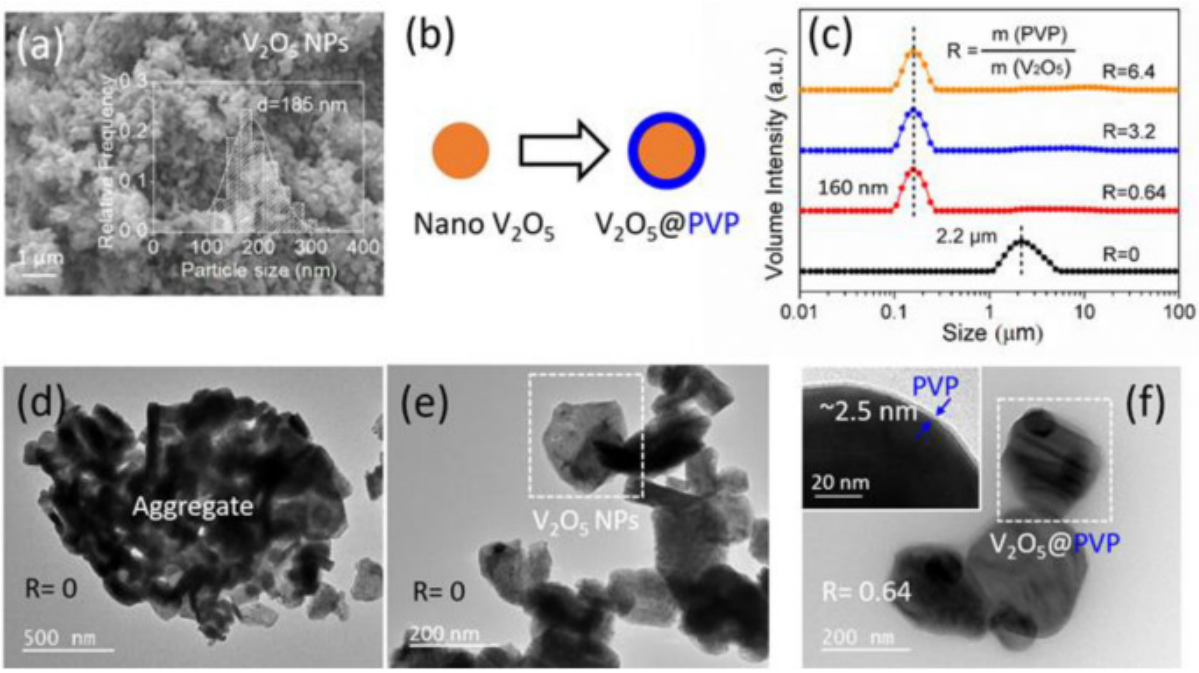

Fig. 1. (a) SEM micrograph and particle size distribution of V2O5 NPs, obtained through ball-milling of V2O5 and soot mixture, followed with a carbon-removing process; (b) Scheme of the core-shell formation of V2O5@PVP; (c) Size distribution in V2O5@PVP suspensions with different weight ratios, R(PVP/V2O5)= 0, 0.64, 3.2, 6.4 (wt); (d, e) HRTEM images of V2O5 NPs before functionalisation with PVP (R= 0) and (f) V2O5@PVP NPs after functionalisation with PVP (R= 0.64)

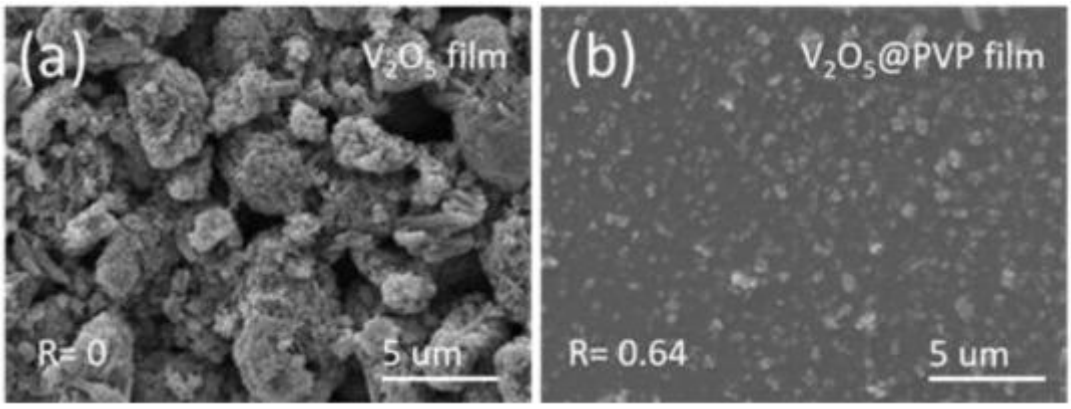

Fig. 2. SEM micrographs of (a) V2O5 film, without PVP addition (R=0); and (b) V2O5@PVP film (R=0.64). The suspension's concentration was fixed to 40 g/L (C40)

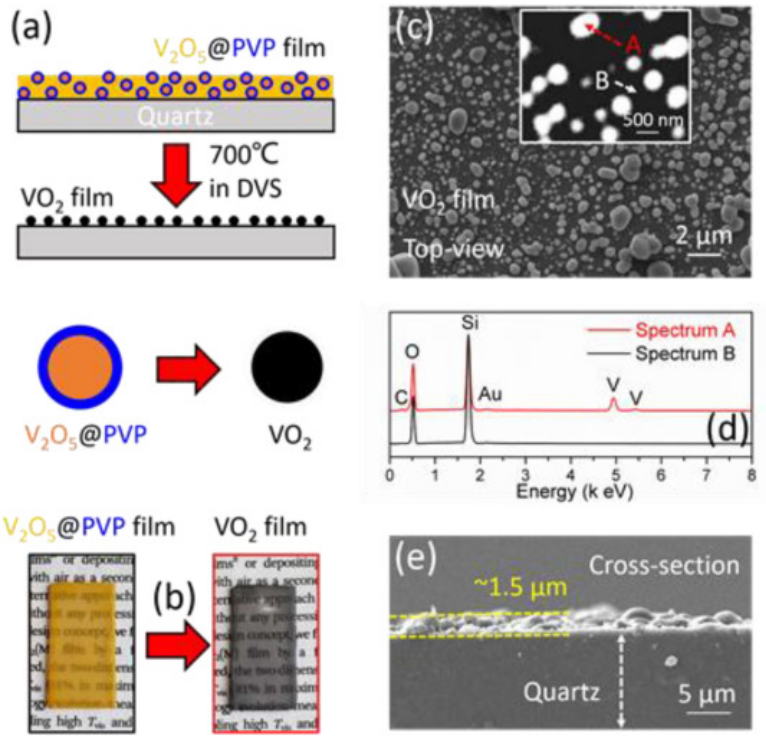

Fig. 3. (a) Schematic representation of the VO2 film preparation from V2O5@PVP film; (b) corresponding film photographs; (c) SEM images of VO2 film on top view and (d) its EDS spectrum of the spot A and B; (e) cross-section view of VO2 film.

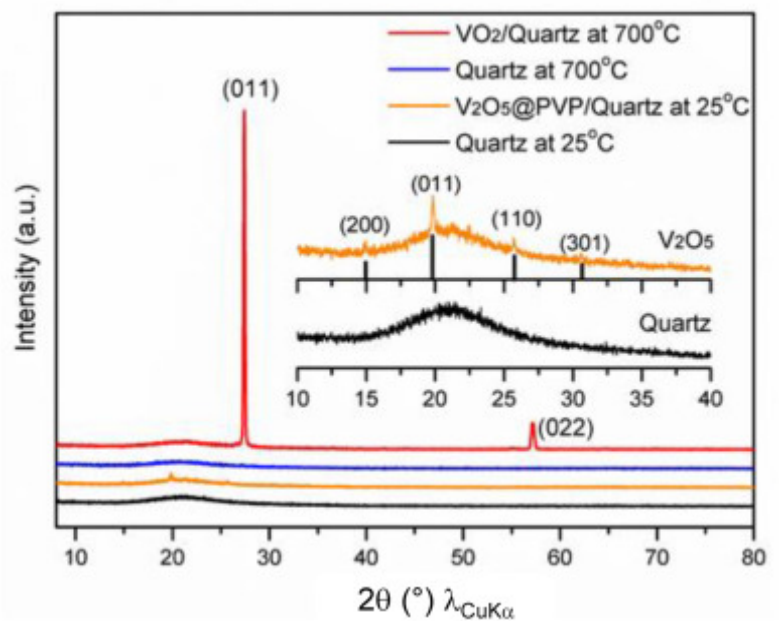

Fig. 4. X-ray diffraction patterns of the quartz substrate, V2O5@PVP/quartz at 25°C, and the quartz substrate and VO2 film/quartz after being annealed at 700°C in dynamic vacuum.

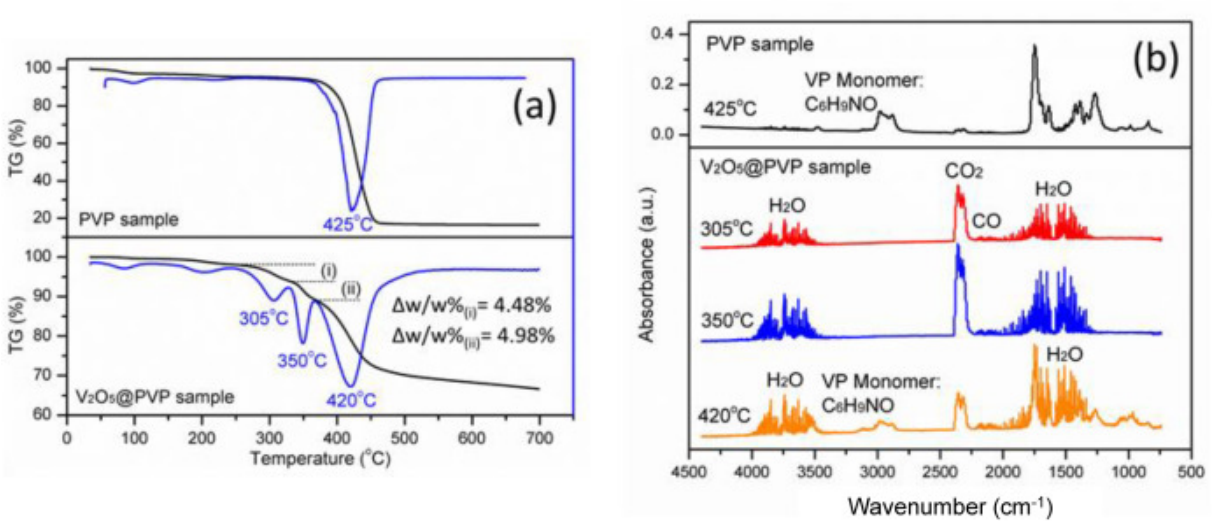

Fig. 5. (a) TG/DTA curves; (b) FTIR spectra of the evolved gas measured at different temperatures for the two samples: pure PVP and V2O5@PVP. The FTIR was recorded in a carrying gas of N2.

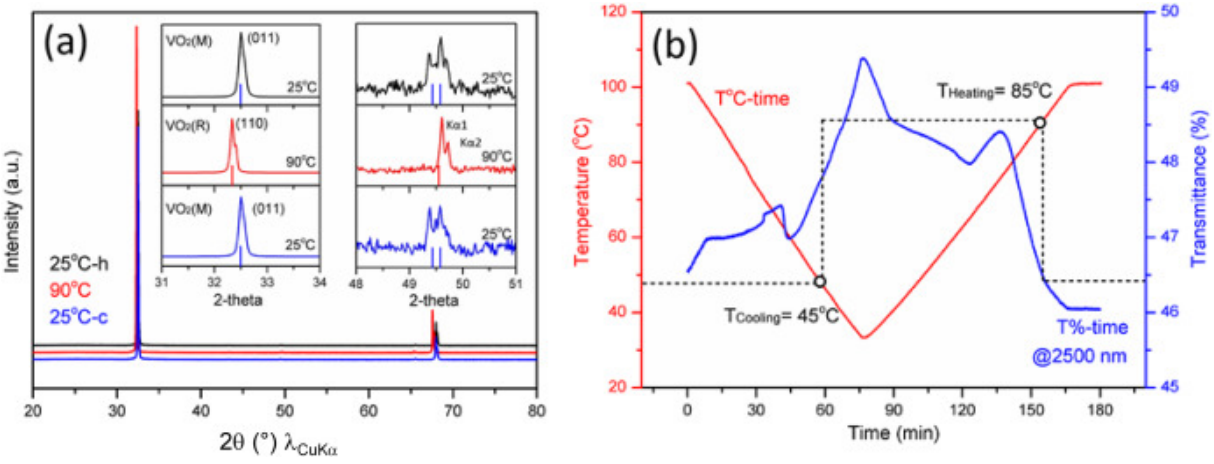

Fig. 6. (a) X-ray diffraction patterns of the as-prepared VO2 film at 25°C and 90°C in the heating cycle (25°C-h, 90°C), and at 25°C in the cooling cycling (25°C-c). Inset, magnification of the 31 to 34° and 48 to 51 °regions.; (b) In-situ transmittance at 2500 nm recorded during cooling and heating of the VO2 film (C80H) (Table 1) in the range of 30-100°C.

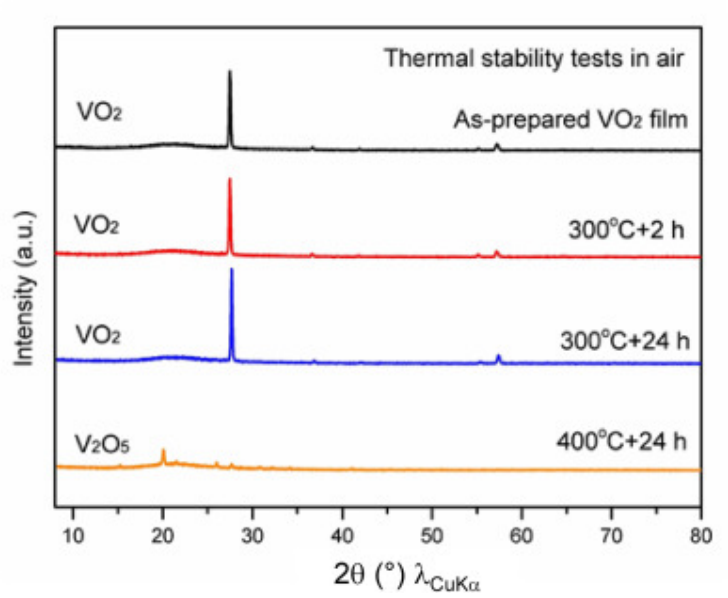

Fig. 7. The X-ray diffraction patterns after thermal stability test of as-prepared VO2 film by annealing at 300°C in air for different durations (0, 2 and 24h), and 400°C for 24h.

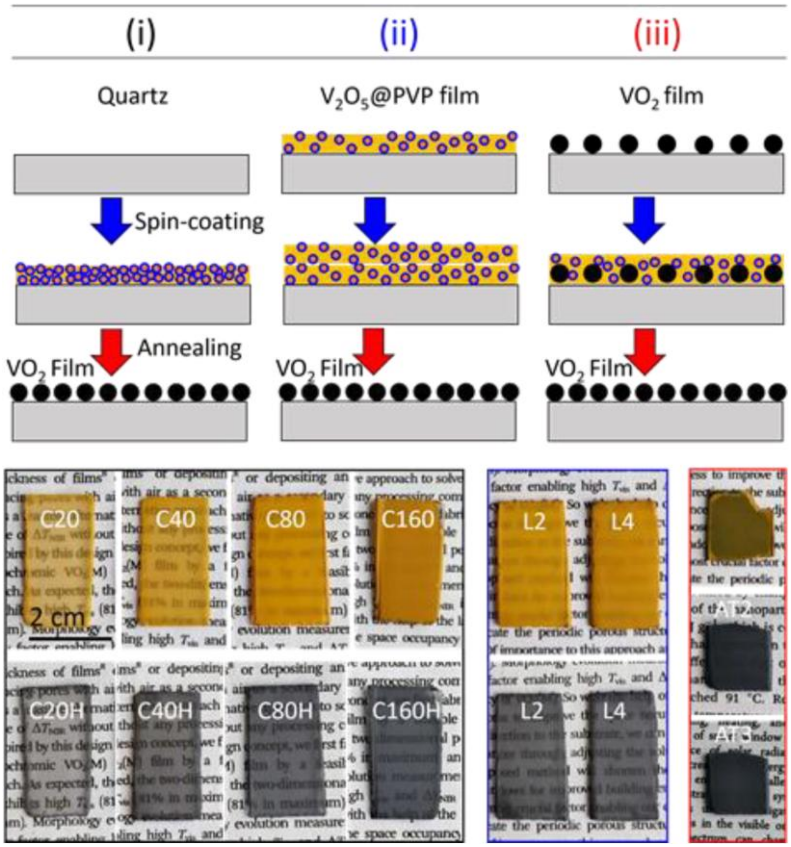

Fig. 8. Scheme of the three methods to increase the surface coverage SC : (i) increase of the V2O5@PVP concentration (20, 40, 80 and 160 g/L) in CHCl3 suspension; (ii) increase of the number of V2O5@PVP layers before a single annealing (2 and 4 layers); (iii) repetition of the spin-coating/annealing process times (2 and 3 times); and the corresponding photographs of V2O5@PVP and VO2 films.

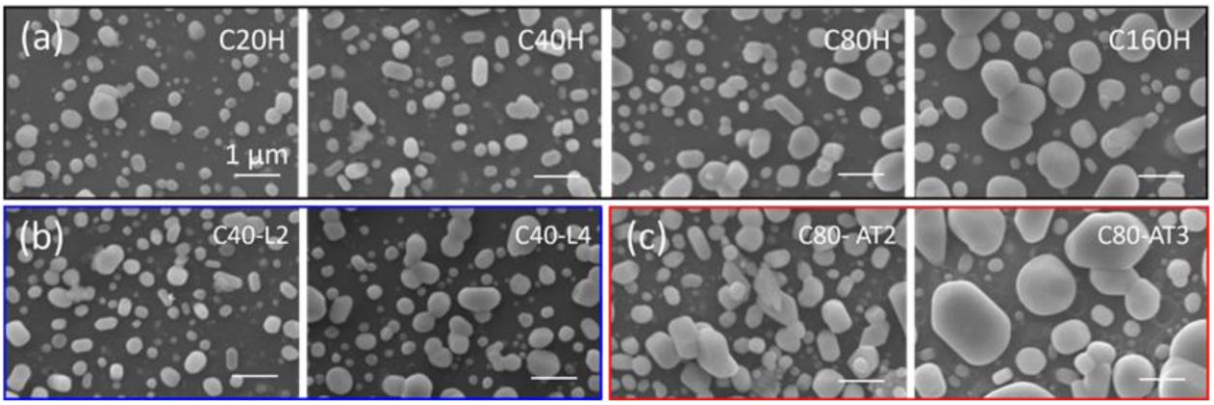

Fig. 9. SEM micrographs of the various as-prepared VO2 films by spin-coating : (a) C20H, C40H, C80H and C160H; (b) L2 and L4; (c) AT2 and AT3.

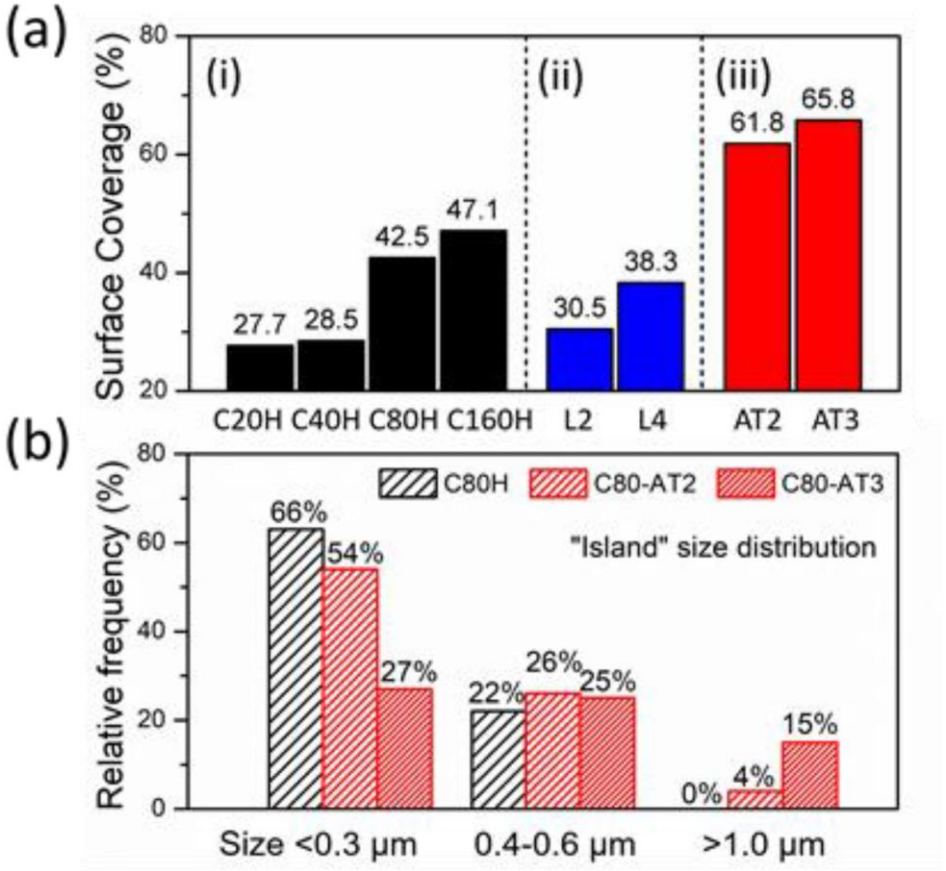

Fig. 10. (a) Surface coverage percentage (SC%) of various VO2 films; (b) “island” size distribution of C80H, C80-AT2, and C80-AT3 samples.

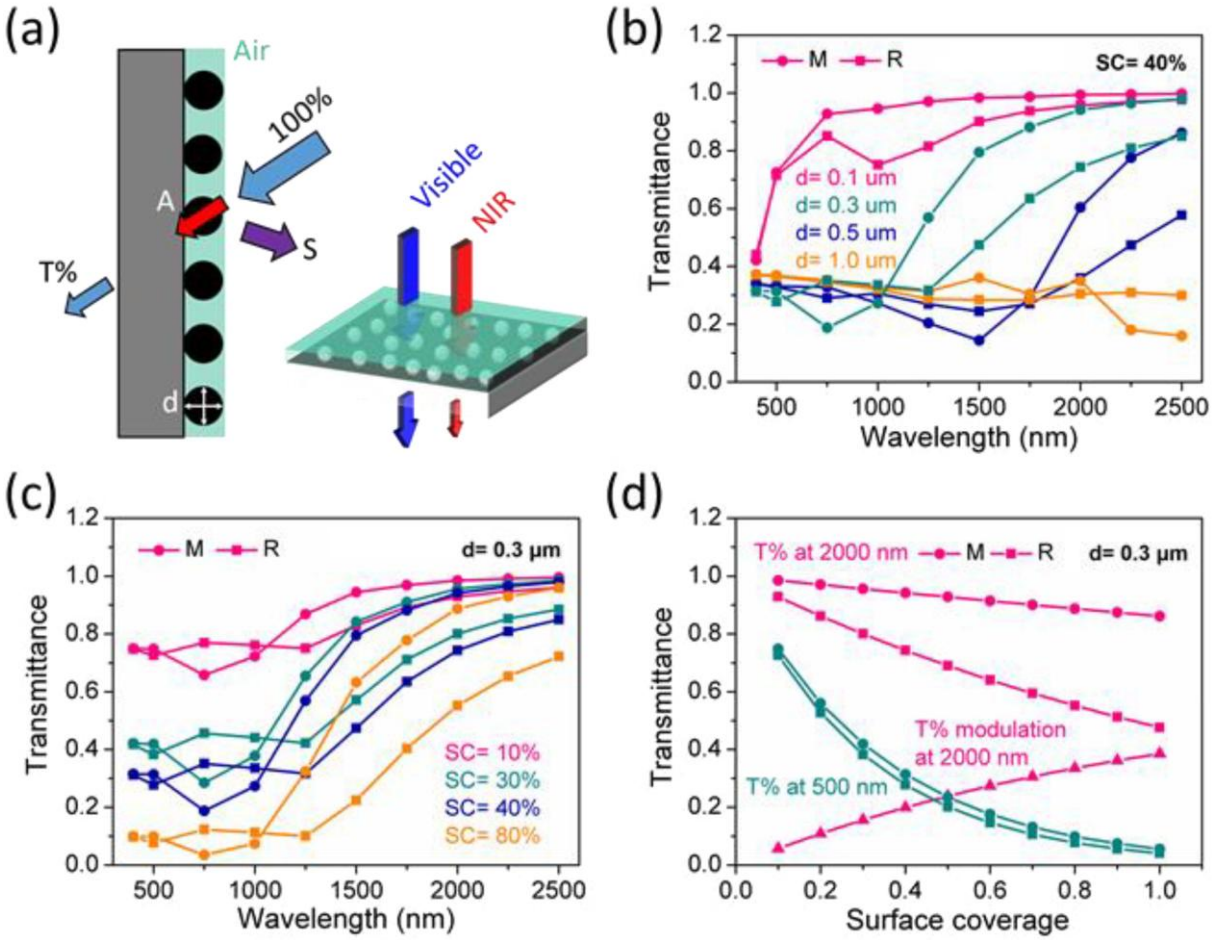

Fig. 11. (a) Schematic illustration of island-shape VO2 film; Simulated transmittance curves for the films (b) under the same surface coverage (SC= 40%) with different particle sizes (d= 0.1, 0.3, 0.5 and 1 micron); and (c) with the same particle size (d= 0.3 micron) under different surface coverages (SC%= 10%, 30%, 40% and 80%); (d) the transmittance values at λ= 500 and 2000 micron extracted from (c).